Huang, A., G. M. Nielson, G. Farin, D. Capco & P. Baluch, Line and net pattern segmentation using shape modeling, *Proceedings of Visualization and Data Analysis 2003*, SPIE Vol. 5009, pp. 171-180, Jan. 2003

Line and net pattern segmentation using shape modeling

Adam Huang[a], Gregory Nielson[a], Anshuman Razdan[b], Gerald Farin[a], David Capco[c], and Page Baluch[c*]

[a] Computer Science and Engineering, [b] PRISM Lab, [c] Biology,
Arizona State University, Tempe, AZ 85287, USA

ABSTRACT

Line and net patterns in a noisy environment exist in many biomedical images. Examples include: Blood vessels in angiography, white matter in brain MRI scans, and cell spindle fibers in confocal microscopic data. These piecewise linear patterns with a Gaussian-like profile can be differentiated from others by their distinctive shape characteristics. A shape-based modeling method is developed to enhance and segment line and net patterns. The algorithm is implemented in an enhancement/thresholding type of edge operators. Line and net features are enhanced by second partial derivatives and segmented by thresholding. The method is tested on synthetic, angiography, MRI, and confocal microscopic data. The results are compared to the implementation of matched filters and crest lines. It shows that our new method is robust and suitable for different types of data in a broad range of noise levels.

Keywords: Image processing, image enhancement, image segmentation, feature extraction, matched filter, crest line, curvature, derivative

1. INTRODUCTION

Line and net patterns in a noisy environment exist in many imaging technologies. Examples include: Roads and rivers in satellite photos, curves in fingerprints, blood vessels in angiography, white matter in brain MRI scans, and cell spindle fibers in confocal microscopic data. Detection of these line and net patterns is important because these features play an essential role in many computerized data analyses. The structure of retinal vessels has measurable abnormalities in diameter, color, and tortuosity which reveal the information on the state of various diseases. The branches of white matter can serve as landmarks for brain registration. The shape and arrangement of spindle fibers provides geometric and topological information for the study and computation of parameters related to cell skeletal mechanisms. Recognition of these patterns provides the very first step in automatic image analysis and computer-aided diagnosis. However, thin structures in biomedical images are intrinsically difficult to recover automatically because they are more vulnerable to noise.

Much of past work on medical image segmentation and early disease detection relied on human interaction to define regions of interests by using methods such as manual editing, regions painting, and interactive thresholding. The drawbacks of such methods are excessive human-interaction time and human-related measurement errors. Therefore, double reading is necessary to reduce the miss rate on radiographic reading. More current approaches have attempted to combine human supervision with automatic analysis. Whether automatic analysis is employed or not, user interaction is well-accepted as being essential in the medical image analysis because the consequences of analysis errors can be catastrophic such as missing a blocked artery in an angiogram.

Computer-aided detection of blood vessels in angiography has been studied for years. At least three different methods have been applied to blood vessel segmentation: Matched filters[1,3], crest lines detection[11], and neural networks[12]. Chaudhuri et al[1] constructed 12 different matched filter templates to detect piecewise linear segments of blood vessels in all possible directions. Gang et al[3] introduced amplitude modified second-order Gaussian filters to improve the detection accuracy of matched filters. Monga et al[11] extracted crest lines by making use of up to the third derivatives. Crest lines are lines where one of the two principal curvatures is locally extremal. Such lines have been used to extract roads in satellite data and blood vessels in medical images. Recently Zana and Klein[20] combined both shape matching and curvature evaluation to segment blood vessels. They highlighted vessels with respect to their

*A.H. | G.N. | A.R. | G.F. | D.C. | P.B.: E-mail: adam.huang | nielson | razdan | farin | dcapco | page.baluch@asu.edu

morphological properties. Vessels were differentiated from analogous background patterns with a cross-curvature evaluation.

Besides of blood vessels, white matter in brain MRI scans, and spindle fibers in a mouse egg confocal microscopic image more or less also share the similar properties of line and net patterns. Extending the existing methods to these images should be straightforward. However, cell spindle images from a confocal microscope[17] are much noisier and remain a challenge to existing methods. A more robust method is needed to extract line and net patterns for data with a broad range of noise levels.

We propose a shape-based modeling method to enhance line and net patterns in biomedical images. Shape-based models generally are abstracted mathematical descriptions or approximations. They have been developed to study and analyze geometric objects from various measurements. The Marching Cubes model[8,14] for volume data, point cloud fitting[5,6] for range images, and active deformable surfaces[7,9,18] for both surface and volume data are just some examples. In addition, shape characteristics have been broadly applied to image and surface analysis. Curvature is a local geometric property for shape description. It is used as an index to analyze and categorize curves and surfaces of archeology artifacts[2]. It is also applied to image and surface segmentation[4,10,17].

In this paper we investigate a semi-automatic segmentation method that takes advantage of the targeted features' distinctive shape characteristics. It is implemented in an enhancement/thresholding type of edge operators. Line and net features are enhanced by partial derivatives based on their abstracted mathematical models. Segmentation is simply implemented by thresholding on the enhanced images. Although user interaction is needed in our approach, users' responsibilities are simply to select proper derivative estimators based on the resulting enhanced images and adjust thresholding value in the thresholding step. The experimental results show that our new method is robust and suitable for different types of data in a broad range of noise levels.

The organization of this paper is as follows. In the second section, we first examine three distinctive characteristics from a retinal image and confirm the fitness of using Gaussian functions as vessel profile approximations. Then, we briefly review matched filters and crest lines methods. In the third section, we first introduce a function model for the line segments that satisfy the three characteristics. Next, we derive and explain why line and net features with a Gaussian-like profile can be enhanced by differential derivatives. Then, we develop an enhancement/thresholding strategy to extract line and net patterns. Experimental results and comparisons are given in the fourth section. Finally, conclusions are presented in the fifth section.

2. BLOOD VESSELS' SHAPE CHARACTERISTICS AND PREVIOUS WORK

As observed in Fig. 1.a, the blood vessels in angiography typically appear as a tree-like pattern. Such a pattern consists of piecewise linear segments with a Gaussian-like profile. By this we mean that the cross section of a blood vessel in a grayscale image $F(x, y)$ appears as a Gaussian distribution function (see Fig. 1.b for example).

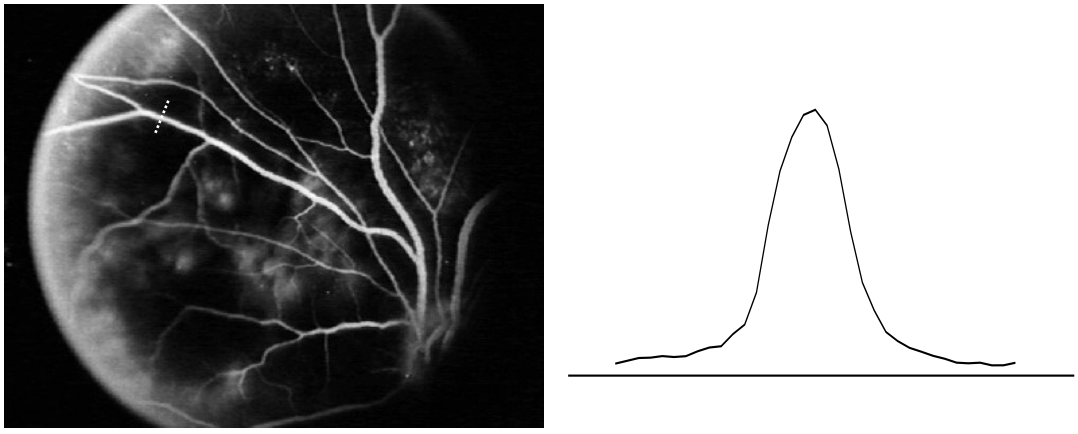

(a) (b)

Figure 1: (a) Fluorescein angiogram obtained from a fundus camera. (b) The grayscale profile of a blood vessel sampled along the dotted line shown in (a).

Chaudhuri et al[1] illustrates three distinctive shape characteristics of blood vessels in retinal images:

1) Blood vessels usually have small curvatures and can be approximated by piecewise linear segments.
2) The grayscale profile along the direction perpendicular to a blood vessel as shown in Fig. 1.b looks like a Gaussian function.
3) The width of a vessel is relatively constant within a range of a few pixels (2 to 10 pixels).

A precise model for blood vessels in angiography is difficult to develop because it varies with many physical factors such as tissue's characteristics, light source, and imaging system's optical and electronic components. However, an approximation that conforms to the principal features and maintains calculation simplicity will be sufficient and acceptable for practical applications. The Gaussian vessel profile is a very popular example. It is generally described by a function similar to

$$f(x,y) = A\{1 \pm k\exp(-d^2/2\sigma^2)\}, \tag{1}$$

where d is the perpendicular distance between the point (x, y) and the axial of the blood vessel, σ defines the spread of the profile, A is the local background intensity, and k is a measure of the relative intensity between the vessel and its neighborhood. In addition to Gaussian vessels, blurred half-elliptical vessels or even simple rectangular vessels have been proposed. It is a valid question to ask how to choose a "good" model.

Gang et al have provided a statistical evaluation in Ref. 3 to prove the fitness of estimating vessel profiles with Gaussian functions. They studied a group of blood vessels that were taken as the green component of color fundus images. Samples of vessels' cross sections were taken and fitted by Gaussian curves with least squares errors criteria. They reported that the relative error ranged from 2% to 5%, averaging at 3.4% in proportion to the amplitude of Gaussian Curves. They also observed that the residual errors were mainly at the periphery. These observations suggest that modeling vessel profiles with Gaussian curves is an appropriate approach.

Now let us consider the detection of blood vessels by using matched filters. The detection of an arbitrary 1D signal $f(\omega)$ through a filter with transfer function $h(\omega)$ has upper limited value using Schwartz's inequality[14]

$$\left|\int_a^b f(\omega)h(\omega)d\omega\right|^2 \le \int_a^b |f(\omega)|^2 d\omega \times \int_a^b |h(\omega)|^2 d\omega . \tag{2}$$

It can be proved that the upper limited value is reached when $h(\omega)$ is equal to $f(\omega)$ multiplied by a constant, that is, $h(\omega) = c \cdot f(\omega)$. This optimal filter is commonly known as matched filter for the signal $f(\omega)$.

When the concept of 1D matched filter is extended to 2D grayscale images, a kernel

$$K(x,y) = \exp\left(-\frac{x^2}{2\sigma^2}\right) \qquad \text{for } |y| \le L/2 \tag{3}$$

is the optimal filter to detect a line segment of Gaussian-like profile located from $(0,-L/2)$ to $(0,+L/2)$ with σ defining the Gaussian profile spread and L the length of the line segment. Similarly, in order to detect a line segment oriented at any angle θ ($0 \le \theta \le \pi$), the kernel is consequently needed to be rotated to all possible angles to search the possible line segment. To strike a balance between computation cost and accuracy, Chaudhuri et al[1] constructed 12 different angled templates to search line segments for all possible directions. Gang et al[3] applied the same method except that they used second-order differential Gaussian filters instead.

While the matched filters approach detecting line segments by the convolution of kernels and grayscale images, the crest lines approach treats the grayscale images as terrain surfaces $(x, y, F(x, y))$. The images are viewed as 3D surfaces and crest lines are the ridges along the "mountain" peaks.

One definition of crest lines proposed in Ref. 3 is: A crest line is a locus of points whose maximal curvature (i.e. maximum absolute value of the two principal curvatures), is a local maximum in the corresponding principal direction. A formula called "extremality", e_m, is derived from the third derivatives of the image:

$$e_m = \nabla k_{\max} \cdot \vec{\mathbf{t}}_{\max} . \tag{4}$$

e_m is the directional derivative of the maximum principal curvature $k_{\max}$ in the corresponding principal direction $\vec{\mathbf{t}}_{\max}$. The principal curvatures and principal directions correspond respectively to the eigenvalues, k_1 and k_2, and the eigenvectors, $\vec{\mathbf{t}}_1$ and $\vec{\mathbf{t}}_2$, of the matrix[13]

$$G = \frac{1}{N}\begin{pmatrix} F_{xx} & F_{xy} \\ F_{yx} & F_{yy} \end{pmatrix}\begin{pmatrix} 1+F_x^2 & F_xF_y \\ F_yF_x & 1+F_y^2 \end{pmatrix}^{-1} \tag{5}$$

where $N = \sqrt{1+F_x^2+F_y^2}$ and the notation F_x and F_{xy} represents partial derivatives. Crest lines are extracted at $e_m = 0$.

3. SHAPED-BASED MODELING AND ENHANCEMENT

As the crest lines approach points out, the "shape" of a line segment in a 2D grayscale image can be observed through a 3D terrain surface (*x*, *y*, *F* (*x*, *y*)). Fig. 2 illustrates the terrain model of blood vessels taken from the central part of Fig. 1.a. Observing any vessel segment from the terrain model in Fig. 2, it resembles a speed bump which is straight and has a Gaussian-like profile and relatively constant width. In other words, the "line" patterns in Fig. 2 satisfy the three shape characteristics described in Sec. 2.

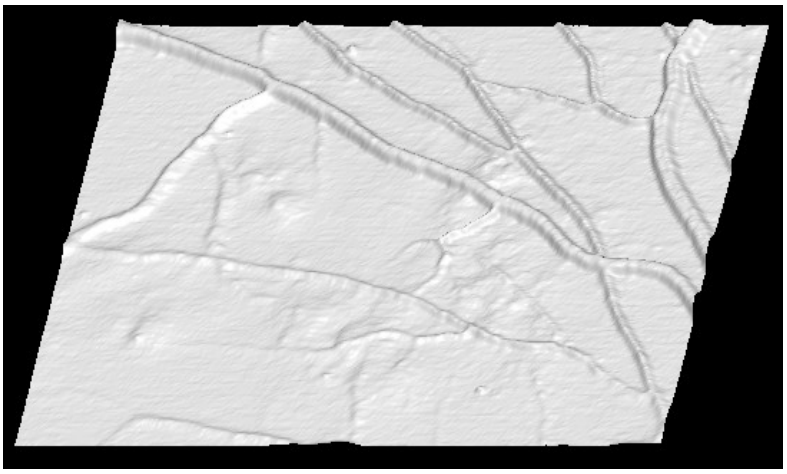

Figure 2: The central patch of the image surface (*x*, *y*, *F* (*x*, *y*)) taken from Figure 1.a .

Since Equation (1) has a mixed look of a function of one variable *d* and two variables *x* and *y*, we define a new function from the terrain surface's viewpoint. A line segment image depicted in Fig. 2 as a terrain surface can be modeled by a function in the neighborhood of an axial point $\mathbf{P}_0$ as

$$F(x,y) = \exp\left(-\frac{[(\mathbf{P}-\mathbf{P}_0)\cdot\mathbf{v}]^2}{2\sigma^2}\right) + C + N(x,y). \tag{6}$$

P is any point (*x*, *y*), $\mathbf{v} = (\cos\theta, \sin\theta)$ is a unit vector perpendicular to the line segment, and σ defines the spread of the Gaussian profile. *C* is the constant noise term and *N* (*x*, *y*) represents the non-constant noise existing at **P**. Assuming the line segment passes through the origin, let $\mathbf{P}_0$ = (0, 0) so that Equation (6) can be modified to

$$F(x,y) = \exp\left(-\frac{(x\cos\theta + y\sin\theta)^2}{2\sigma^2}\right) + C + N(x,y). \tag{7}$$

The second derivatives of $F(x, y)$ are

$$F_{xy}(x,y) = F_{yx}(x,y) = -\frac{\cos\theta\sin\theta}{\sigma^2}\exp\left(-\frac{(x\cos\theta + y\sin\theta)^2}{2\sigma^2}\right) + \frac{\cos\theta\sin\theta}{\sigma^4}(x\cos\theta + y\sin\theta)^2\exp\left(-\frac{(x\cos\theta + y\sin\theta)^2}{2\sigma^2}\right) + N_{xy}(x,y) \quad (8)$$

$$F_{xx}(x,y) = -\frac{\cos^2\theta}{\sigma^2}\exp\left(-\frac{(x\cos\theta + y\sin\theta)^2}{2\sigma^2}\right) + \frac{\cos^2\theta}{\sigma^4}(x\cos\theta + y\sin\theta)^2\exp\left(-\frac{(x\cos\theta + y\sin\theta)^2}{2\sigma^2}\right) + N_{xx}(x,y) \quad (9)$$

$$F_{yy}(x,y) = -\frac{\sin^2\theta}{\sigma^2}\exp\left(-\frac{(x\cos\theta + y\sin\theta)^2}{2\sigma^2}\right) + \frac{\sin^2\theta}{\sigma^4}(x\cos\theta + y\sin\theta)^2\exp\left(-\frac{(x\cos\theta + y\sin\theta)^2}{2\sigma^2}\right) + N_{yy}(x,y) \quad (10)$$

To obtain an enhanced image from the second derivatives, we first form a matrix

$$\mathbf{H} = \begin{bmatrix} F_{xx} & F_{xy} \\ F_{yx} & F_{yy} \end{bmatrix}. \quad (11)$$

The noise terms $C+N$ (x, y) in Equation (7) will diminish faster than the signal through the differential operator by two well-known processes. The high frequency noise will be minimized by the smoothing process of derivative estimation. The differential operator will remove low frequency noise such as the constant and ramp components. Accordingly, noise terms N_{xx} , N_{xy}, and N_{yy} in Equations (8), (9), and (10) will be less significant and can be neglected. In addition, the second terms of these equations can be omitted if $x\sin\theta + y\cos\theta$ is much smaller than σ. Therefore,

$$\begin{aligned} \mathbf{Hv} &\approx -\frac{1}{\sigma^2}\exp\left(-\frac{(x\cos\theta + y\sin\theta)^2}{2\sigma^2}\right)\begin{bmatrix} \cos^2\theta & \cos\theta\sin\theta \\ \cos\theta\sin\theta & \sin^2\theta \end{bmatrix}\begin{bmatrix} \cos\theta \\ \sin\theta \end{bmatrix} \\ &= -\frac{1}{\sigma^2}\exp\left(-\frac{(x\cos\theta + y\sin\theta)^2}{2\sigma^2}\right)\begin{bmatrix} \cos\theta \\ \sin\theta \end{bmatrix} \\ &= \lambda(x,y)\mathbf{v}. \end{aligned} \quad (12)$$

λ is an eigenvalue of matrix **H** and **v** is the corresponding eigenvector. Since **v** is perpendicular to the line segment, λ must be the maximum absolute eigenvalue. **H** is the Hessian Matrix. The enhanced image is defined as

$$\overline{F}(x,y) = \begin{cases} -\sigma^2\lambda(x,y) & \text{if } \lambda(x,y) < 0 \\ 0 & \text{if } \lambda(x,y) \geq 0 \end{cases} \quad (13)$$

(a) (b) (c)

Figure 3: (a) Original blood vessel image. (b) Enhanced image. (c) Extracted vessel patterns by thresholding on the enhanced image.

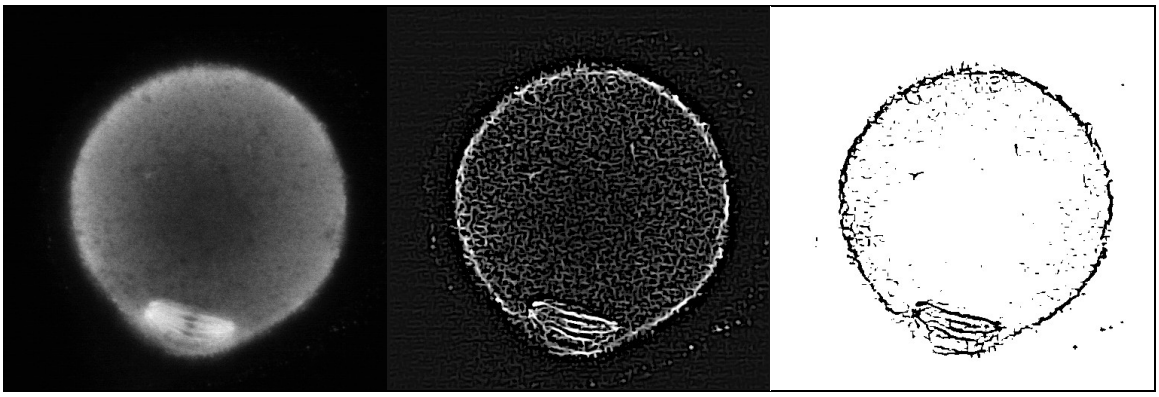

(a) (b)

Figure 4: (a) Original mouse egg spindle image from a confocal microscope. (b) Enhanced image. (c) Extracted fiber patterns by thresholding on the enhanced image.

As the spread of line patterns is usually unknown at the processing time or the lines have various spreads, σ in Equation (13) can be either omitted or assigned a default value.

So far, we have derived an enhancement process from the function model described in Equation (7) by using second derivatives. Finally, we develop a two-stage algorithm to extract the line and net patterns:

1) Estimate the second derivatives from the original image and synthesize an enhanced image by Equation (13).
2) Extract the thin line patterns simply by thresholding on the enhanced image.

The extracted line and net patterns are collections of pixels at which the enhanced image $\overline{F}(x, y)$ is larger than or equal to the thresholding value. Although more sophisticated data structures and representations can be derived from these pixel sets, for the explanatory purpose and computational simplicity we will maintain the algorithm as an enhancement/thresholding type of operators. The extraction process is illustrated in Fig. 3 and 4.

Fig. 3.a, 3.b, and 3.c show the original, enhanced images, and extracted patterns of blood vessels in an angiogram respectively. The original and enhanced data are shown as grayscale images. Since the extracted patterns are simply sets of pixels, they are illustrated as black pixels in Fig. 3.c. Fig. 4 basically describes the same procedure which is applied to a very different data set. Fig. 4.a is a mouse egg image obtained from a confocal microscope. The main focus in this image is to extract the line structure from the barrel-shaped spindle positioned at the lower membrane. These lines are clear in the central region and seem to fuse into one piece of cloud at either pole. In spite of the very different appearance between angiography and confocal microscopy, our method was able to extract both blood vessels and cell spindle fibers successfully. Furthermore, as observed in Fig. 4.b, our method was able to enhance and reveal detailed line features other than the spindle fibers that are barely noticeable in the original image.

4. EXPERIMENTAL RESULTS AND COMPARISONS

We have tested our new method on four data sets with line and net patterns from different sources. The images include: a circular line pattern with a Gaussian profile calculated from mathematical formulas, an angiogram obtained from a fundus camera, a slice of brain MRI scans, and a mouse egg spindle image from a fluorescence confocal microscope. The experimental results are shown in Fig. 5 to 8. The original data sets are illustrated in grayscale images and the extracted line and net patterns is represented by sets of black pixels at which the enhanced image values are larger than or equal to the thresholding value. The results are compared to the implementation of matched filters and crest lines.

The images produced by the crest lines and matched filters methods may contain extra structures such the center of the concentric rings in Fig. 5.c and short branches from blood vessels in Fig. 7.b. They may miss other parts such the intersections of lines in Fig. 5.c and 6.c. The reason of these differences is because a very simple discriminator, thresholding, is applied in deciding whether a pixel belongs to a targeted structure or not. It is not easy to find an appropriate thresholding value to separate line and net patterns from the background noise. If we threshold the processed

data with a lower thresholding value, we obtain not only more targeted structures but also false parts as the result of noise. If we raise the thresholding value, we remove more noise with the cost of losing some information. As we mention in the previous section, more sophisticated data structures can be derived from the extracted pixel sets and therefore, more information such as diameter and length can be added into the decision criteria. In spite of the simplicity, our algorithm produces consistent and clean results for different types of data regardless of the noise level.

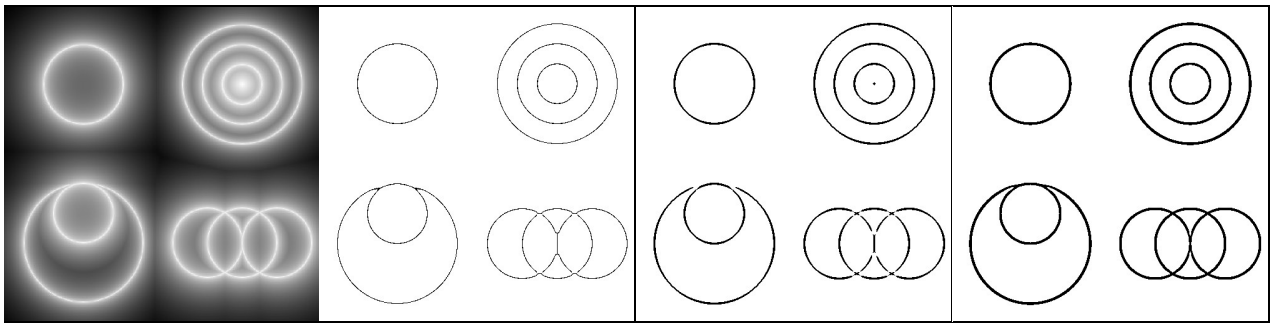

(a) (b) (c) (d)

Figure 5: (a) A synthetic line pattern with a Gaussian-like profile. (b) Crest lines extraction. (c) Matched filters enhancement/ thresholding. (d) Shape models enhancement/thresholding.

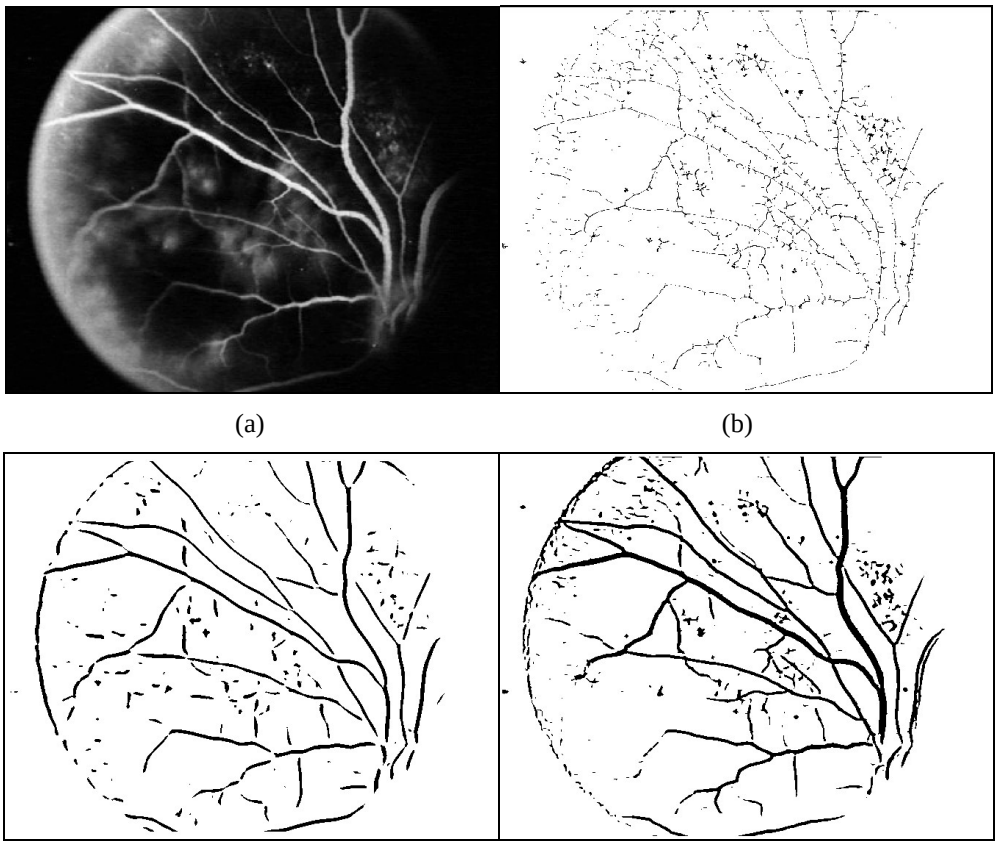

(a) (b)

(c) (d)

Figure 6: (a) Fluorescein angiogram. (b) Crest lines extraction. (c) Matched filters enhancement/ thresholding. (d) Shape models enhancement/thresholding.

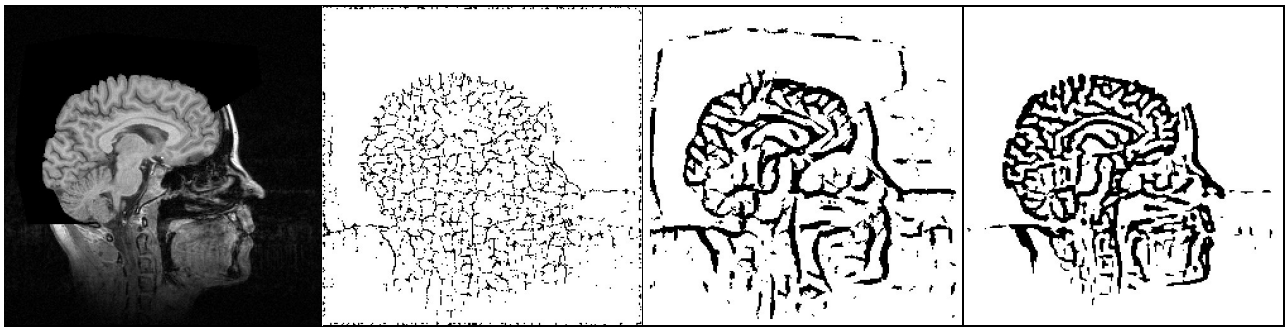

(a) (b) (c) (d)

Figure 7: (a) Brain MRI image. (b) Crest lines extraction. (c) Matched filters enhancement/ thresholding. (d) Shape models enhancement/thresholding.

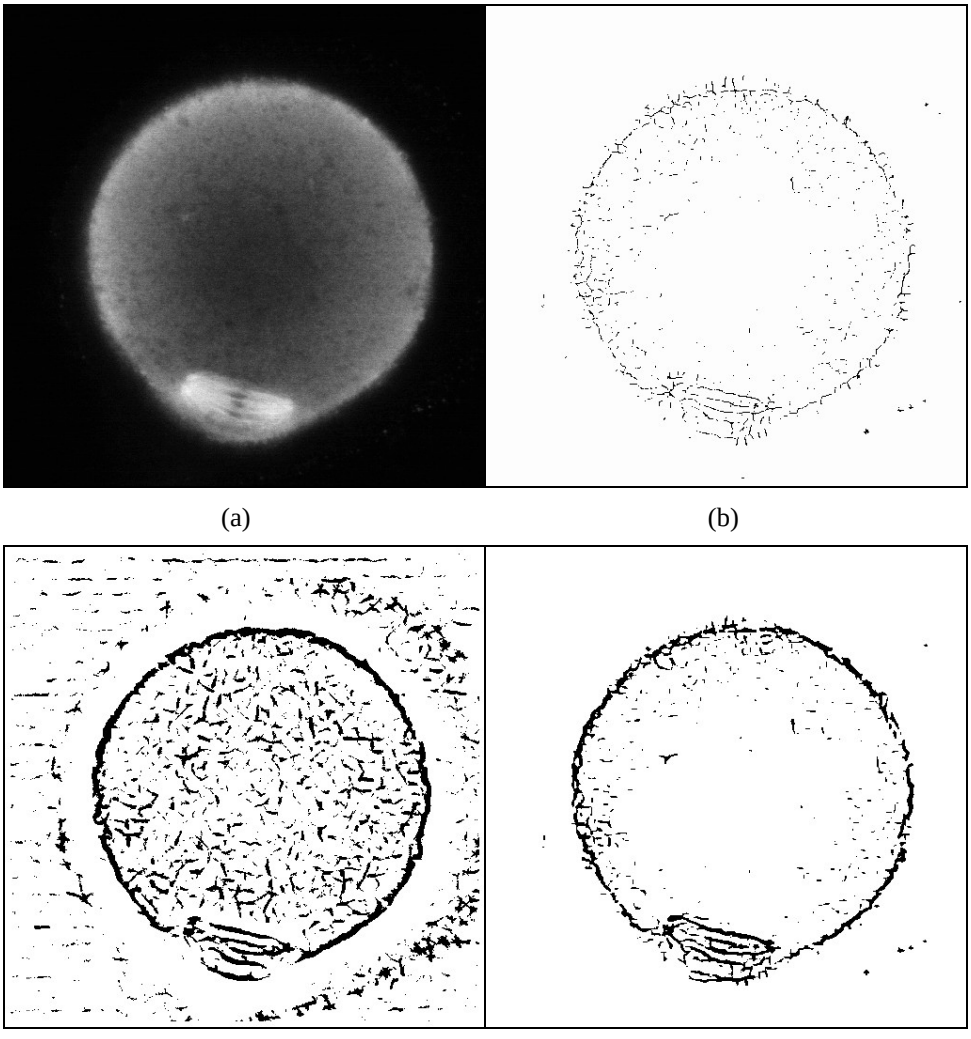

(a) (b)

(c) (d)

Figure 8: (a) Mouse egg confocal microscopic image. (b) Crest lines extraction. (c) Matched filters enhancement/thresholding. (d) Shape models enhancement/thresholding.

5. CONCLUSIONS

We have introduced a shape-based modeling and enhancement method to extract line and net patterns by take advantage of their distinctive shape characteristics. From the proposed shape model, we provide an explanation of using the maximum eigenvalue from Hessian Matrix as an enhanced image. The proposed extraction scheme retains the computational simplicity of an enhancement/threshodling type of edge operators. Although it is possible to combine existing methods to build more sophisticated data structures from the extracted pixel sets to obtain information such as diameter, length, and connectivity for accuracy improvement, our algorithm was able to extract line and net patterns from various types of imaging technologies by simply thresholding on the enhanced images. Compared to matched filters and crest lines methods, the shaped-based modeling and enhancement method proves to build a robust algorithm that is suitable for different types of images in a broad range of noise levels. From angiography, MRI, to confocal data, it performs well in analyzing various line and net patterns emerged in various noise levels. With some modifications, this method could be extended to the extraction of ecological features from satellite images and the enhancement of fingerprints rather easily. Our future work is to extend the Gaussian-profile shape model to 3D data sets with line and thin layer patterns.

ACKNOWLEDGMENTS

This research was supported by NFS IIS-9980166 & ACI-0083609, ONR N00014-00-1-0281, and DARPA MDA972-00-1-0027. The blood vessel image is from the Bristol BioMedical Image Archive, University of Bristol, UK. It is provided as a courtesy of Professor Lawrence Hirst at Princess Alexandra Hospital, Brisbane. The brain MRI data is from Stanford Computer Graphics Laboratory Volume Data Archives. It is provided as the courtesy of Siemens Medical System, Inc. Iselin, NJ. Data was edited (skull removed) by Dr. Julian Rosenman, North Carolina Memorial Hospital. The first author would like to thank J. Hu and P. Mongkolnam for numerous discussions and inspiration.

REFERENCES

1. S. Chaudhuri, S. Chatterjee, N. Katz, M. Nelson, and M. Goldbaum, “Detection of blood vessels in retinal images using two-dimensional matched filters,” in *IEEE Transactions on Medical Imaging*, vol. 8, no. 3, pp. 263-269, September 1989.
2. G. Farin, “Shape,” in *Mathematics Unlimited -2001 and Beyond*, B. Engquist and W. Schmid, eds., Springer-Verlag, pp. 463-466, 2001.
3. L. Gang, O. Chutatape, and S. M. Krishnan, “Detection and Measurement of Retinal Vessels in Fundus Images Using Amplitude Modified Second-Order Gaussian Filter,” in *IEEE Transactions on Biomedical Engineering*, vol. 49, no. 2, pp. 168-172, February 2002.
4. W. E. Higgins and E. J. Ojard, “Interactive Morphological Watershed Analysis for 3D Medical Images,” in *Computer Medical. Imaging Graphics*, Special Issue on Advanced 3D Processing in Medicine, 17(4/5), pp. 387-392, 1993.
5. H. Hoppe, T. DeRose, T. Duchamp, J. McDonald, and W. Stuetzle, “Surface Reconstruction from Unorganized Points,” in *Proceedings of SIGGRAPH ’92*, pp. 71-78, July 1992.
6. A. Huang and G. M. Nielson, “Surface Approximation to Point Cloud Data Using Volume Modeling,” to appear in *Data Visualization*, F. Post, G. Nielson, and G. P. Bonneau eds., Elvesier Pub., 2002.
7. M. Kass, A. Witkin, and D. Terzopoulos, “Snakes: Active Contour Models,” in *Int’l J. of Computer Vision*, pp. 321-331, 1988.
8. W. E. Lorensen and H. E. Cline, “Marching Cubes: A High Resolution 3D Surface Construction Algorithm,” in *Computer Graphics*, vol. 21, no. 4, pp. 163-169, July 1987.
9. R. Malladi, J. A. Sethian, and B. C. Vemuri, “Shape Modeling with Front Propagation: A Level Set Approach,” in *IEEE Transactions on Pattern Analysis and Machine Intelligence*, vol. 17, no. 2, February 1995.
10. A. P. Mangan and R. T. Whitaker, “Partitioning 3D Surface Meshes Using Watershed Segmentation,” in *IEEE Transactions on Visualization and Computer Graphics*, vol. 5, no. 4, pp. 308-321, 1999.
11. O. Monga, N. Armande, and P. Montesinos, “Thin nets and crest lines: Application to satellite data and medical images,” in *Proceedings, International Conference on Image Processing*, pp. 468-471, January 1995.
12. R. Nekovei and Y. Sun, “Back-propagation network and its configuration for blood vessel detection in angiograms,” in *IEEE Transactions on Neural Networks*, vol. 6, pp. 64-72, January 1995.

13. G. M. Nielson, T. A. Foley, B. Hamann, and D. Lane, “Visualizing and Modeling Scattered Multivariate Data,” in *IEEE Computer Graphics and Applications*, vol.11, no. 3, pp.47-55, May 1991.
14. G. M. Nielson, A. Huang, and S. Sylvester, “Approximating Normals for Marching Cubes Applied to Locally Supported Isosurfaces,” in *Proceedings of IEEE Visualization 2002*.
15. A. Papoulis, *Signal Analysis*, McGraw-Hill, New York, 1977.
16. S. Pulla, A. Razdan, and G. Farin, “Improved Curvature Estimation for Watershed Segmentation of 3-Dimensional Meshes,” submitted to *IEEE Transactions on Visualization and Computer Graphics.*
17. A. Razdan, K. Patel, G. E. Farin, and D. G. Capco, “Volume Visualization of Multicolor Laser Confocal Microscope Data,” in *Computers and Graphics*, vol. 25, no 3, 2001.
18. D. Schlesinger, J. Snell, L. Mansfield, J. Brookeman, J. Ortega, and N. Kassell, “Segmentation of Volumetric Medical Imagery Using Multiple Geodesic-based Active Surfaces,” in *SPIE Proc.* **2710**, pp. 243-253, 1996.
19. L. Vincent and P. Soille, “Watersheds in Digital Spaces: An Efficient Algorithm Based on Immersion Simulations,” in *IEEE Transactions on Pattern Analysis and Machine Intelligence*, vol. 13, no. 6, pp. 583-598, June 1991.
20. F. Zana and J. C. Klein, “Segmentation of Vessel-like Patterns Using Mathematical Morphology and Curvature Evaluation,” in *IEEE Transactions on Image Processing*, vol. 10, no. 7, pp. 1010-1019, July 2001.